

# Unraveling the solidification path of a *pahoehoe* “cicirara” lava from Mount Etna volcano

Gabriele Lanzafame · Silvio Mollo · Gianluca Iezzi · Carmelo Ferlito · Guido Ventura

Received: 13 July 2012 / Accepted: 23 February 2013 / Published online: 26 March 2013  
© Springer-Verlag Berlin Heidelberg 2013

**Abstract** The solidified surface of a lava flow reflects the viscosity of its molten fraction and the crystal content during flow; crystal-poor basaltic lavas produce *pahoehoe* fields, whereas crystal-rich ones solidify with *aa* carapaces. At Mount Etna, volcano *aa* morphologies are very common, whereas *pahoehoe* lavas are rare. The latter are locally named “cicirara” due to the presence of centimeter-sized plagioclase phenocrysts much more abundant than in *aa* lavas. The phenocryst content of “cicirara” lavas contrasts with the low viscosity generally associated with *pahoehoe* morphology. Therefore, to reconcile the discrepancy between textural and volcanic observations, we have studied the most primitive *pahoehoe* “cicirara” lava sampled until now. Two samples at 0.5 and 1 m from the bottom of the 2-m thick lava flow were investigated on the basis of their mineral compositional variations and textural features, i.e., size frequency and crystal size distribution (CSD). Results coupled with rheological models indicate that only large phenocrysts of plagioclase (>1 mm) and clinopyroxene have grown before eruption. Thermobarometric models and petrological computations based on the composition of plagioclase and clinopyroxene phenocryst cores highlight that only a small amount (10–15 vol.%) of crystals equilibrated

at 12 km of depth. Cumulative size frequency and CSD data also indicate that plagioclase and clinopyroxene phenocryst rims grew heterogeneously and coalesced around their cores at depths <1 km, before eruption. In this view, the “cicirara” lava was erupted with a low crystalline content that favoured the formation of its *pahoehoe* surface; however, crystals with a size <1 mm (~75 vol.%) solidified at post-eruptive conditions. Our findings underline that the emplacement of high-viscosity *aa* or low-viscosity *pahoehoe* lavas is driven by the degree of undercooling imposed by the volatile exsolution rate in the shallowest portion of the Etnean plumbing system. A slow magma ascent rate promotes significant intratelluric degassing and widespread nucleation; consequently, the viscosity of the suspension significantly increases leading to an *aa* morphology. In contrast, *pahoehoe* “cicirara” lavas are associated with a rapid rise to the surface of poorly degassed, undercooled magmas.

**Keywords** Pahoehoe lava · “Cicirara” · Mount Etna · CSD · Thermobarometers

## Introduction

At Mount Etna volcano *pahoehoe* primitive lavas are less common than *aa* (Branca et al. 2011). Generally, *pahoehoe* types are (1) primary if a lava flow has an extensive, typically smooth, billowy or ropy crust from vent to the distal zone and (2) secondary if they are erupted at the margin of *aa* lavas (Chester et al. 1985; Kilburn and Guest 1993; Guest et al. 2012). As frequently determined for Hawaiian lava flows, the formation of a *pahoehoe* surface is produced by the low (1) viscosity of suspension, (2) terrain slope, (3) output and strain rate (Cashman et al. 1999; Hon et al. 2003; Kilburn 2004; Iezzi and Ventura 2005; Soule and Cashman 2005; Guest et al. 2012). Moreover, the content and the shape of crystals determine the formation of basic lava

Editorial responsibility: M.R. Patrick

G. Lanzafame · C. Ferlito  
Dipartimento di Scienze Biologiche, Geologiche e Ambientali,  
Università di Catania, Corso Italia 57,  
95129 Catania, Italy

S. Mollo · G. Iezzi · G. Ventura  
Istituto Nazionale di Geofisica e Vulcanologia,  
Via di Vigna Murata 605,  
00143 Rome, Italy

G. Iezzi (✉)  
Dipartimento INGEO – Ingegneria e Geologia,  
Università G. d’Annunzio, Via Dei Vestini 30,  
66013 Chieti, Italy  
e-mail: g.iezzi@unich.it

crusts and their rheological properties. In particular, low amounts of crystals with more equant shapes favour *pahoehoe* morphologies (Hoover et al. 2001) that, in turn, are not dictated by the absolute crystal size (Saar et al. 2001). The influence of the strain rate and the ground slope on the morphology of *pahoehoe* lavas at Mount Etna have been the topic of previous studies (Chester et al. 1985; Kilburn and Guest 1993; Guest et al. 2012) that confirmed the general observations described above. Conversely, the importance of crystallization on the formation of *pahoehoe* morphologies is quite unknown (Hughes et al. 1990). In light of this, it is notable that the majority of primary *pahoehoe* lava flows at Mount Etna contain centimeter-sized plagioclases, locally named “cicirara” lavas because of their chick-pea like appearance. “Cicirara” lavas were erupted several times during the evolution of the volcano, especially from the intermediate to final activity of the Ellittico eruptive center (since 15 ka) and in the 17th century (Chester et al. 1985; Nicotra and Viccaro 2012). On the whole, *pahoehoe* lavas show (1) bulk and mineral compositions comparable to the majority of Etnean products erupted since 15 ka, (2) a porphyric index >40 vol.%, and (3) a great amount (>34 vol.%) of centimeter-sized plagioclases. Moreover, these *pahoehoe* lavas outcrop in many sectors of the volcano and their peculiar texture has been interpreted as the result of a long residence time of magma in a shallow reservoir (Guest et al. 1984; Hughes et al. 1990; Corsaro and Pompilio 2004; Nicotra and Viccaro 2012).

There is general consensus that basaltic Hawaiian lavas develop *pahoehoe* morphologies (1) when the lava suspension (crystal content <25–30 vol.%) attains a yield strength at the Newtonian–Binghamian transition (Cashman et al. 1999; Hoover et al. 2001; Saar et al. 2001; Hon et al. 2003) and (2) when the critical shear rate is not continuously exceeded (Kilburn 2004). This critical shear rate increases as the bulk viscosity decreases. Since Hawaiian *pahoehoe* lavas are less viscous than Etnean ones (Kilburn 2004), the maximum crystal content measured for *pahoehoe* Hawaiian lavas represents a conservative limit for Etnean *pahoehoe* morphologies. Notably, primitive lavas show *aa* morphologies only for crystal contents >35 vol.% (Cashman et al. 1999; Hoover et al. 2001). This explains the major presence of *aa* lavas at Mount Etna and underlines that “cicirara” lavas can be erupted only with a low amount of intratelluric crystals.

To clarify the relationship between morphology and crystal texture of “cicirara” lavas, we have investigated several pre-historic to historic *pahoehoe* lava flows. Then, we have selected the most primitive “cicirara” lava (CICG1) analyzed until now, whose composition is also close to that of Hawaiian *pahoehoe* lavas. Textural and chemical features of this lava were used for determining the crystal size frequency, crystal size distribution (CSD) and crystallization conditions. Results indicate that (1) phenocryst cores crystallized

at a depth of 12 km, (2) phenocryst rims mainly grew during magma ascent at a depth <1 km below the vent, and (3) microphenocrysts and microlites formed at sub-aerial conditions. This reconstruction provides an alternative explanation with respect to previous models suggesting *pahoehoe* “cicirara” lavas were erupted with a high crystal content.

### Sampling and analytical methods

“Cicirara” lavas were occasionally erupted during the 17th century. They were frequently associated with lateral eruptions at different elevations on the flanks of the volcanic edifice of Mount Etna. The locations of the “cicirara” lavas in this study are displayed in Fig. 1. In agreement with their *pahoehoe* character, “cicirara” lavas form extensive, broad lava flow fields. We collected 15 rock samples from eight different lava fields of the pre-historic and historic activities (Table 1 and Fig. 1). XRF whole-rock analyses were performed at the University of Catania (Table 1). Results are plotted in Fig. 2 and compared with other “cicirara” lavas from previous studies. The studied lava flow units have thickness from 1 to 5 m; we selected two sub-samples since (a) the cooling condition at 0.5 and 1 m from the bottom of this lava during its emplacement could not be identical and (b) to enlarge the statistical relevance of textural and micro-chemical data. These two sub-samples are

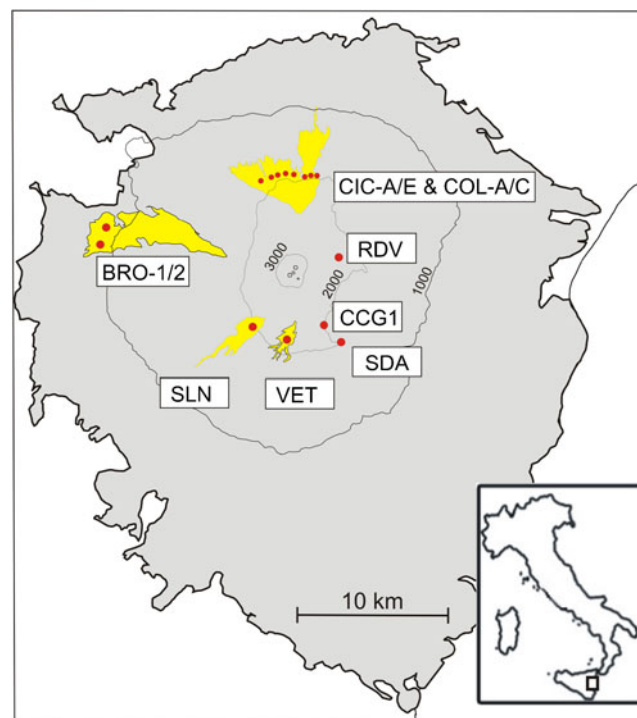


**Fig. 1** “Cicirara” *pahoehoe* lava flows (yellow) investigated in this study and their locations (red circle). The composition of these samples and their ages are reported in Table 1

**Table 1** Major element compositions of “cicirara” lava flows

Sample	COL-A	COL-B	COL-C	CIC-A	CIC-B	CIC-C	CIC-D	CIC-E	BRO-1	BRO-2	VET	SLN	SDA	RDV	CICGI
Age	1614–1624	1614–1624	1614–1624	1614–1624	1614–1624	1614–1624	1614–1624	1614–1624	1651	1651	1985	1610	prehistoric	prehistoric	prehistoric
SiO <sub>2</sub>	50.18	50.15	50.04	50.68	50.40	50.38	50.97	51.14	49.42	49.81	49.76	50.43	52.50	52.40	49.99
TiO <sub>2</sub>	1.58	1.58	1.58	1.58	1.59	1.57	1.54	1.56	1.61	1.60	1.60	1.52	1.44	1.40	1.64
Al <sub>2</sub> O <sub>3</sub>	18.18	18.23	18.00	18.18	18.21	18.57	19.12	18.87	17.38	17.44	18.28	18.30	19.48	19.94	17.61
FeO <sub>tot</sub>	9.60	9.52	9.59	9.39	9.45	9.18	8.78	8.94	10.17	9.98	10.29	9.60	8.53	8.03	9.31
FeO	7.90	7.56	7.35	7.30	7.35	7.20	7.30	7.00	6.80	6.80	7.80	7.58	7.98	7.40	6.20
Fe <sub>2</sub> O <sub>3</sub>	2.56	2.18	2.49	2.46	2.48	2.43	2.39	2.42	2.19	2.37	2.63	2.67	2.57	2.43	2.03
MnO	0.17	0.18	0.18	0.17	0.18	0.17	0.17	0.17	0.19	0.19	0.18	0.17	0.16	0.15	0.18
MgO	3.53	3.61	3.83	3.37	3.51	3.30	2.72	2.85	4.54	4.38	3.55	3.45	1.97	2.02	5.17
CaO	10.24	10.44	10.76	10.15	10.24	10.22	9.71	9.66	11.45	11.12	10.79	11.13	9.11	8.18	10.31
Na <sub>2</sub> O	4.03	3.98	3.82	4.04	4.02	4.14	4.33	4.27	3.55	3.66	3.39	3.28	4.06	4.74	3.72
K <sub>2</sub> O	1.81	1.82	1.73	1.84	1.85	1.87	1.96	1.93	1.58	1.61	1.59	1.59	1.82	2.15	1.79
P <sub>2</sub> O <sub>5</sub>	0.55	0.50	0.47	0.56	0.53	0.53	0.57	0.57	0.41	0.44	0.55	0.45	0.61	0.69	0.56
L.O.I.	0.00	0.00	0.00	0.00	0.00	0.00	0.00	0.28	0.00	0.00	0.95	0.58	0.51	1.53	0.00
Tot	100.00	100.00	100.00	100.00	100.00	100.00	100.00	100.00	100.00	100.00	100.00	100.00	100.00	100.00	100.00
Mg# <sup>a</sup>	46.25	46.84	48.16	45.5	46.18	45.69	41.75	42.84	50.55	50.47	44.24	45.5	34.82	37.09	53.26

<sup>a</sup> Mg# = Mg/(Mg+Fe) in mole fractions

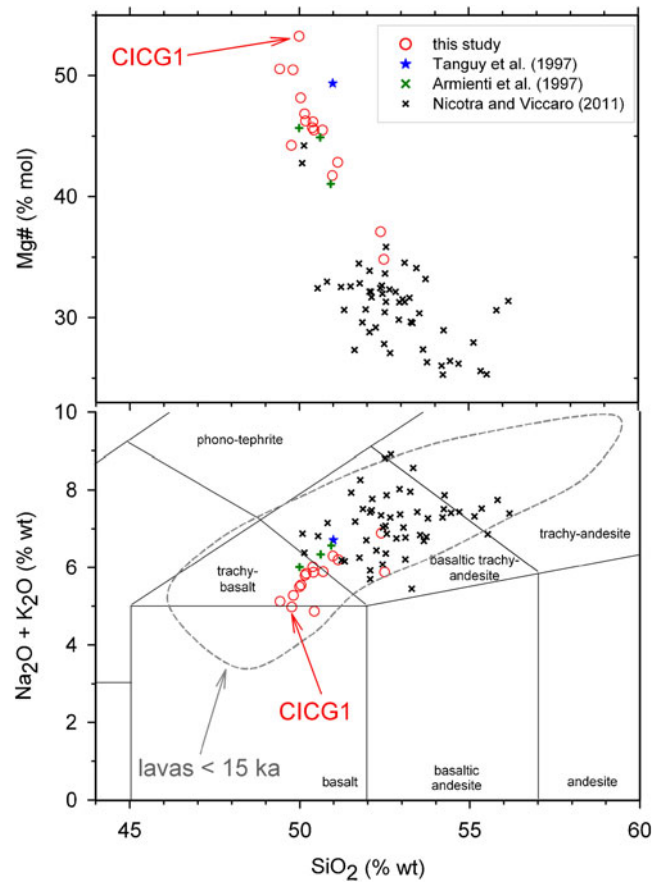
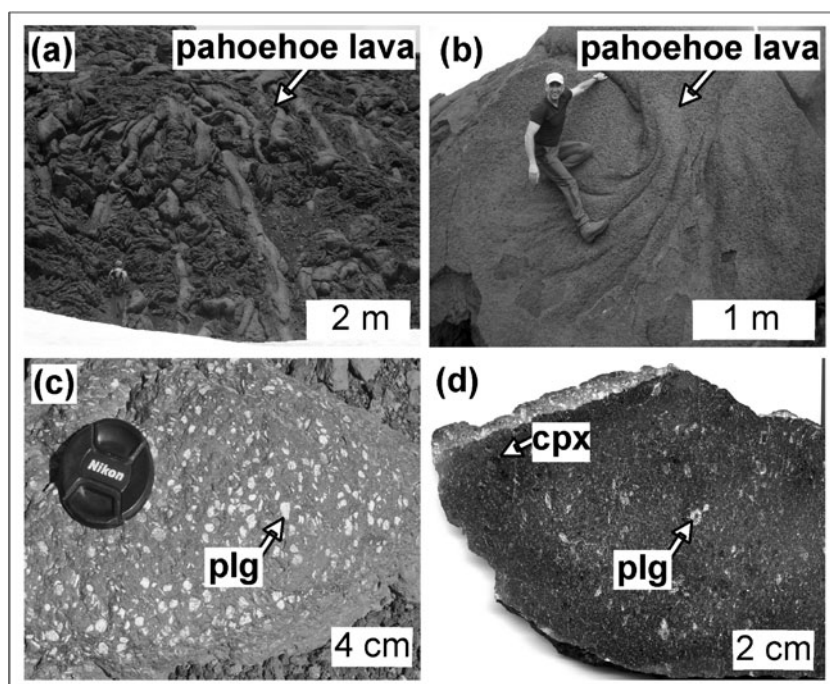


**Fig. 2** Na<sub>2</sub>O+K<sub>2</sub>O vs. SiO<sub>2</sub> and Mg# vs. SiO<sub>2</sub> diagrams. Samples from this study and from literature are reported. Etnean lavas younger than 15 ka are from Ferlito and Lanzafame (2010)

characterized by the presence of centimeter-sized plagioclase with irregular shapes and vesicle contents <5 vol.% always concentrated at the outermost lava portions; The most representative features that are observable in the field and in hand-specimen samples are displayed in Fig. 3.

In this study, we focus on the textural and chemical features of the most primitive “cicirara” lava flow sampled until now, i.e., CICG1 lava (Fig. 2). To do this we have collected two sub-samples at about 0.5 and 1 m from the bottom of this lava flow with a thickness of 2 m. The chemistry and the texture of minerals were studied with a Jeol-JXA8200 (EPMA-WDS) and a Jeol FE-SEM 6500F (SEM-EDS) at the INGV of Rome (Italy), following the protocols described by Iezzi et al. (2008). Representative chemical analyses for each phase are reported in Table 2. According to Armienti et al. (1994a), quantitative textural analyses were obtained at three different magnifications, in order to consider the differences between largest and smallest crystals. Phenocrysts with the longest size >4 mm have a relatively low number density and thus we measured them directly on polished rock samples with an area of 1.5 × 10<sup>4</sup> mm<sup>2</sup>. Crystals with length <4 and >0.1 mm, and <0.1

**Fig. 3** Prehistoric *pahoehoe* “cicirara” lavas with typical smooth (a) to ropy (b) crust morphologies. The two CICG1 sub-samples were collected from a single flow unit. Mesoscopic specimens (c and d) show the presence of typical millimetric to centimetric crystals of plagioclase and clinopyroxene. Notably, the irregular shape of large plagioclase crystals is also evidenced



and  $>0.005$  mm were measured on backscattered images with an area of 150 and  $1.67$  mm<sup>2</sup>, respectively. The image analysis and phase segmentation were performed with Image Pro Plus software. SEM backscattered images were transformed in grey scale for determining the abundance, aspect ratio and dimension of each phase. An example of phase segmentation and size frequency determination at intermediate magnification is reported in Fig. 4. Since crystal impingement occurred only for plagioclase microlites, we slightly ( $<5$  vol.%) reduced the areas of such microlites, taking advantage of the lighter grey tone of their rims ( $1\text{--}2$   $\mu\text{m}$ ). The area of each mineral phase was then binarized with different colors (Fig. 4) and, successively, each crystal phase was counted (Table 3). The shortest and longest crystal axes were determined as the best-fitting ellipse of a bi-dimensional crystal section following Higgins (2006) and Iezzi et al. (2011). The crystal habit of each phase was estimated using the CSD-slice software implemented by Morgan and Jerram (2006) (Table 3). The CSD for plagioclase, clinopyroxene and titanomagnetite populations was calculated with CSD-Corrections 1.38 package, using the 2D longest dimension and the crystal habit (Higgins 2000, 2006). CSD plots of plagioclase were constructed by integrating all the textural measurements obtained at large, intermediate and small magnifications; whereas, those of clinopyroxene and titanomagnetite were determined from SEM images. CSD plots are characterized by a number of points for each phase in excess of 3,500, 1,700 and 500 for plagioclase, clinopyroxene and titanomagnetite, and a relatively low amount of 6, 5 and 4 bins per decade, respectively (Higgins 2000, 2006; Armienti 2008). In

agreement with previous studies (Armienti et al. 1984; Murphy et al. 2000), phenocrysts, microphenocrysts and microlites have been discriminated on the basis of the longest size dimensions  $>0.3$ ,  $0.3\text{--}0.1$ , and  $<0.1$  mm, respectively (Table 3).

## Results

In general, *pahoehoe* “cicirara” lavas vary within a limited compositional range from trachybasalt to basaltic trachyandesite (Fig. 2). Although Nicotra and Viccaro (2012) have reported more evolved compositions for “cicirara” lavas (Fig. 2), these were characterized by *aa* crusts and not *pahoehoe* morphologies. In this study, we have studied in depth the CICG1 sample, the most primitive ( $\text{Mg}\#=53.26$ ) *pahoehoe* “cicirara” lava (Table 1 and Fig. 2) with a holocrystalline texture and rare bubbles ( $<1$  vol.%) in the dark matrix (Fig. 5). The total amount of phenocrysts, microphenocrysts and microlites is 31–35, 9–9 and 60–57 vol.%, respectively (Table 3). Glomeroporphyritic clusters (0.5–5 mm of 3–15 attached crystals) of clinopyroxene, olivine, titanomagnetite and plagioclase are common, and plagioclase and clinopyroxene frequently host tiny crystals of titanomagnetite and/or olivine (Fig. 5).

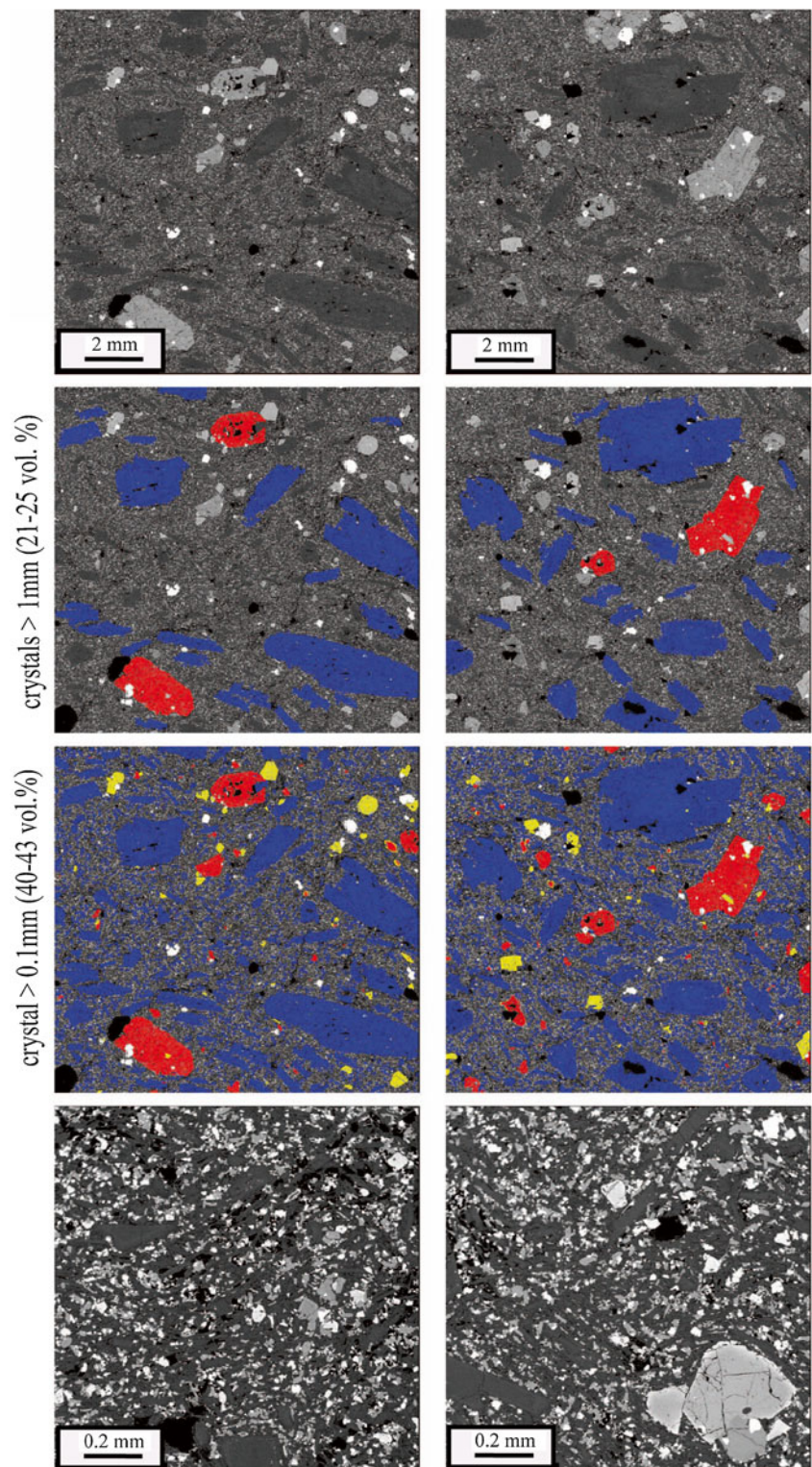
Plagioclase is the most abundant mineral, followed by clinopyroxene and minor titanomagnetite and olivine crystals; notably, the abundance of plagioclase in the groundmass is lower than that measured for the phenocryst and microphenocryst populations (Table 3). Only the innermost part of the plagioclase (and clinopyroxene) phenocryst cores is homogeneous in composition, representing a total bulk



Table 2 (continued)

	Olivine			Microclites	titanomagnetite			Microclites								
	Phenocryst cores	Phenocryst rims and microphenocrysts	Microclites		Phenocryst rims and microphenocrysts	Microclites	Microclites									
SiO <sub>2</sub>	38.35	37.97	38.24	37.96	37.51	37.79	35.97	35.96	37.28	SiO <sub>2</sub>	0.10	0.08	0.04	0.14	0.13	0.15
FeO	21.07	21.79	22.54	22.77	23.56	24.18	34.15	33.63	26.00	TiO <sub>2</sub>	12.64	11.13	10.50	19.15	18.85	18.23
MnO	0.56	0.55	0.58	0.63	0.68	0.71	1.15	1.04	0.64	Al <sub>2</sub> O <sub>3</sub>	6.35	6.69	6.58	2.29	2.33	2.84
MgO	38.73	38.31	37.34	37.34	36.80	35.90	28.20	28.31	34.61	FeO	75.82	77.09	76.90	75.34	75.48	75.29
CaO	0.43	0.46	0.52	0.51	0.55	0.55	0.52	1.00	0.55	MnO	0.51	0.47	0.29	0.78	0.83	0.76
Total	99.14	99.08	99.22	99.20	99.10	99.13	99.99	99.94	99.07	MgO	4.09	4.09	5.19	1.42	1.55	1.93
									CaO	0.06	0.03	0.00	0.14	0.11	0.12	
									Cr <sub>2</sub> O <sub>3</sub>	0.00	0.00	0.02	0.01	0.00	0.01	
									Total	99.56	99.57	99.52	99.26	99.29	99.32	
<i>Cations on the basis of 4 oxygens</i>																
Si	1.003	0.998	1.006	1.001	0.995	1.004	0.999	0.997	1.001	Si	0.002	0.001	0.001	0.002	0.002	0.002
Fe <sup>2+</sup>	0.461	0.479	0.496	0.502	0.523	0.537	0.793	0.780	0.584	Ti	0.158	0.139	0.131	0.240	0.236	0.228
Mn	0.012	0.012	0.013	0.014	0.015	0.016	0.027	0.024	0.014	Al	0.124	0.131	0.129	0.045	0.046	0.056
Mg	1.510	1.501	1.465	1.468	1.456	1.422	1.167	1.171	1.385	Fe <sup>3+</sup>	0.000	0.000	0.000	0.000	0.000	0.000
Ca	0.012	0.013	0.015	0.014	0.016	0.016	0.016	0.030	0.016	Fe <sup>2+</sup>	1.055	1.073	1.070	1.049	1.051	1.048
										Mn	0.007	0.007	0.004	0.011	0.012	0.011
										Mg	0.102	0.101	0.129	0.035	0.038	0.048
										Ca	0.001	0.000	0.000	0.002	0.002	0.002
										Cr	0.000	0.000	0.000	0.000	0.000	0.000
Fo	76.62	75.81	74.71	74.52	73.58	72.58	59.54	60.01	70.36	Usp	38.36	33.83	30.21	55.78	54.73	53.37
Fa	23.38	24.19	25.29	25.48	26.42	27.42	40.46	39.99	29.64	FeO mol%	55.98	55.3	53.54	59.98	59.72	59.36
										Fe <sub>2</sub> O <sub>3</sub> mol%	27.41	29.79	32.02	18.05	18.53	19.31
										TiO <sub>2</sub> mol%	16.61	14.91	14.44	21.96	21.74	21.33

**Fig. 4** Textural features and related image analyses of the CIGG1 sub-samples collected at 0.5 (*left*) and 1 (*right*) m from the bottom of the lava. The *first*, *second* and *third* rows show the SEM images at low magnification, and related phase segmentations for crystal lengths  $>1$  and  $>0.1$  mm; the *fourth* row shows the SEM images at high magnification. Plagioclases, clinopyroxenes, olivines and titanomagnetite are shown in *blue*, *red*, *yellow* and *white*, respectively



volume of 10–15 vol.% in the samples. Plagioclase phenocrysts display a maximum length of 15 mm and vary from 26 to 28 vol.% (Table 1). Their cores, especially those of largest crystals, are generally surrounded by plagioclase microlites and this agglomeration feature is also evident in the field (Figs. 3c and 5). The largest plagioclases are

equant, but show irregular shapes mainly due to incipient or near-complete agglomeration of smaller plagioclases along their longest axes (Figs. 3c–d and 5). Both phenocrysts ( $An_{76-61}$ ) and microphenocrysts ( $An_{60-51}$ ) are normally zoned (Table 3), whereas plagioclase microlites show the lowest An contents ( $An_{54-43}$ ).

**Table 3** Textural features of the two analyzed sub-samples

Crystal length (mm)	Plagioclase (vol.%)	Clinopyroxene (vol.%)	Olivine (vol.%)	Titanomagnetite (vol.%)	Total (vol.%)
> 10	2–3	–	–	–	2–3
> 7	6–9	–	–	–	6–9
> 3	11–14	–	–	–	11–14
> 1	19–22	2–3	–	–	21–25
> 0.3 (phenocrysts)	26–28 (1:1.9–3:3.8–3.9)	3–4 (1:1.5–1.6:2.2–3.3)	1–1 (1:1.3–1.4:1.5–2.8)	1–1 (1:1.2:1.6)	31–34
> 0.1	35–37 (1:2–2.5:3.7–4.8)	3–4 (1:1.2–1.6:3.6–4)	1–1 (1:1.3–1.4:1.5–2.8)	1–1 (1:1.1:1.8–1.9)	40–43
< 0.1 (microlites)	43–42 (1:1.5–1.8:3.2–3.7)	10–9 (1:1.4:2.7–2.8)	1–1 (1:1.6:3.3)	6–5 (1:1.3:1.7–1.9)	60–57
average crystal shape	(1:1.8–2.0:3.6–4.0)	(1:1.3–1.4:2.8–3.3)	(1:1.7:3.3)	(1:1.3:1.7–1.9)	(1:1:1.3)

Values on the left and on the right are from the sample at 0.5 and 1 m from the bottom of the CIG1 lava, respectively. Values reported in brackets are the crystalline shapes

Clinopyroxene phenocrysts are 3–4 vol.% with a maximum length of 3 mm. They are sub-euhedral to anhedral and frequently enclose titanomagnetite and olivine. Clinopyroxenes show salitic to diopsidic compositions, with a high content of tschermak components, especially in microlites (Tables 2 and 3 and Fig. 5). Phenocrysts and microphenocrysts are normally zoned showing Si–Mg–Ca-rich cores surrounded by Al–Fe<sup>3+</sup>–Ti-rich rims (Table 2); similar to plagioclase phenocrysts, only the innermost portion of these cores is chemically homogeneous.

Olivine phenocrysts (1 vol.%) have a maximum length of 0.8 mm (Table 3). Larger crystals are frequently resorbed, whereas smaller ones are subrounded in shape (Fig. 5). Olivine shows normal zoning from core (Fo<sub>77-75</sub>) to rim (Fo<sub>75-72</sub>); in contrast, groundmass microlites (1–1 vol.%) are unzoned, varying from Fo<sub>70</sub> to Fo<sub>59</sub> (Table 2).

Titanomagnetite is frequently hosted in phenocrysts of olivine, clinopyroxene and plagioclase (Fig. 4). Titanomagnetite phenocrysts (1 vol.%) are generally Usp-poor and Mg-rich relative to groundmass microlites (Table 2).

CSD plots of plagioclase, clinopyroxene and spinel of the CIG1 sub-samples are displayed in Fig. 6. Similar trends are observable for the same mineral phase although some differences are due to variable phase abundances (Table 3). The CSD slopes decrease as the crystal size increases and the CSD curves became flat as the crystal dimension increases, i.e., the number densities of minerals do not follow a constant log-linear trend (Fig. 6). Notably, plagioclase and, to a less extent, clinopyroxene have three distinguishable slopes. Trends of plagioclase break at about 0.1 and 1 mm, as quantitatively measured by the linear regression analysis of the log-linear

**Fig. 5** Textural features of plagioclase (*plg*), clinopyroxene (*cpx*), titanomagnetite (*timt*) and olivine (*ol*). The plagioclase occurs as large zoned sieve-textured crystals (a and b). Olivine and titanomagnetite are frequently enclosed in clinopyroxene (c). Glomeroporphyritic clusters of minerals are also common in all samples (d)

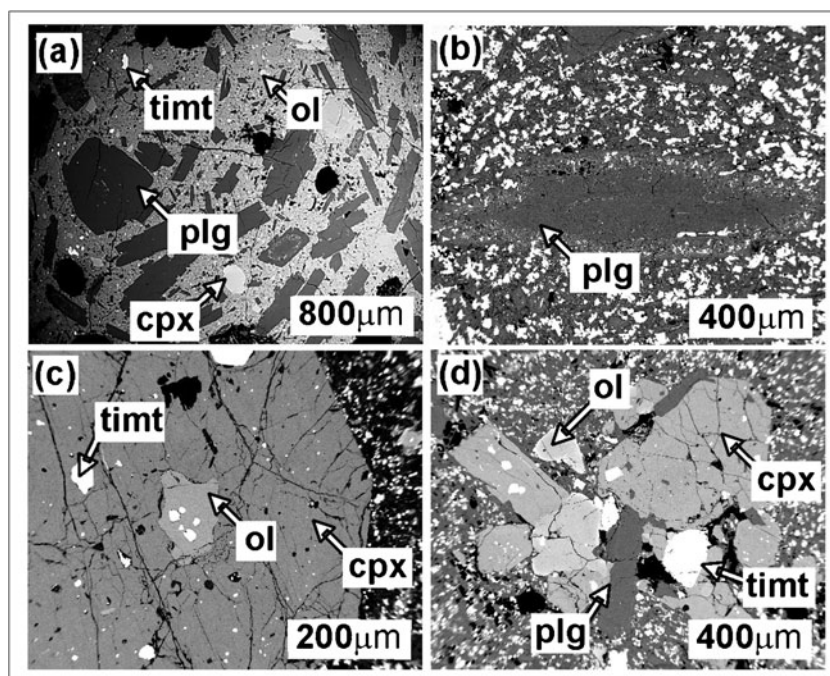
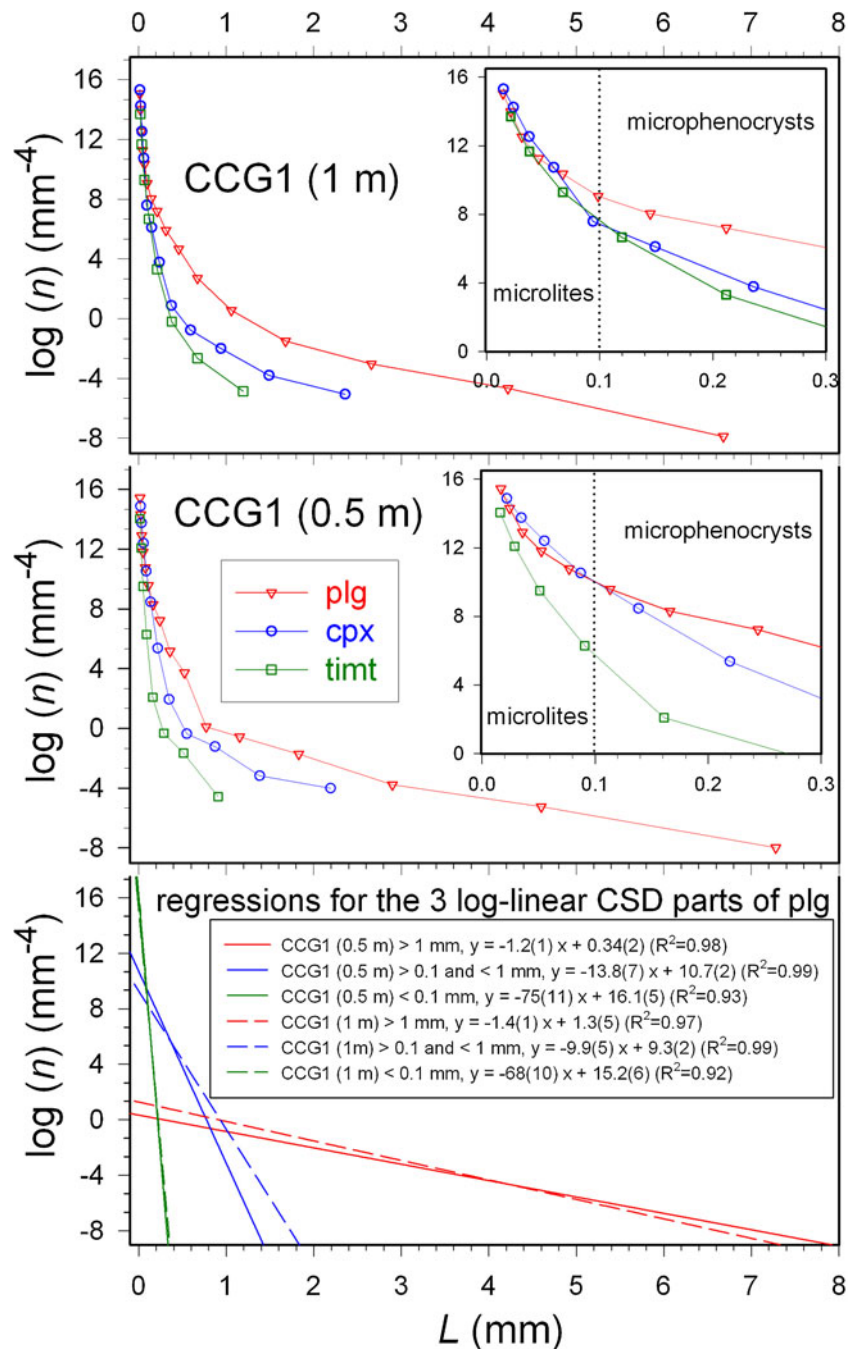




**Fig. 6** CSD plots of plagioclase (*plg*), clinopyroxene (*cpx*), titanomagnetite (*timt*) and relative log-linear regression and fitting results. Data refer to CCG1 sub-samples collected at 0.5 and 1 m from the bottom of this lava. The CSD insets highlight the trends obtained at smaller crystal sizes



part of CSD (Fig. 6). It is worth noting that plagioclase CSD trends depicted in Fig. 6 are also very similar to those reported by Armienti et al. (1997) for two historical “cicirara” lavas.

**Discussion**

**Intratelluric crystallization**

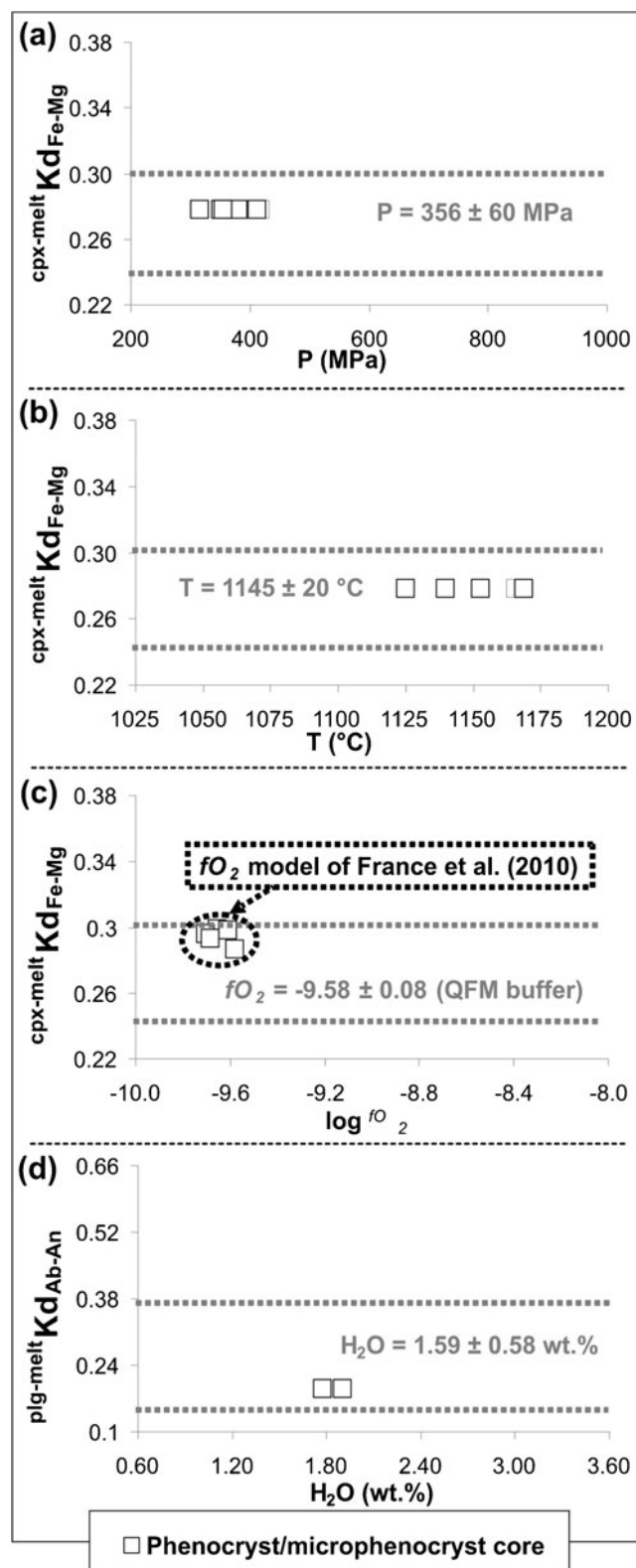
Several investigations based on experiments and natural rock samples have demonstrated that the liquid line of descent of

the trachybasalt to trachyandesite Etnean magmas is mainly dictated by the crystallisation of plagioclase and clinopyroxene (Tanguy et al. 1997; Metrich and Rutherford 1998; Corsaro and Pompilio 2004; Del Gaudio et al. 2010). Accordingly, we have used the compositions of these two minerals to constrain the  $P-T-H_2O-fO_2$  crystallisation conditions. In fact, Etnean magmas do not significantly differentiate with time (Fig. 2); therefore, the composition of intratelluric crystal cores is generally in equilibrium with that of the starting melt (Mollo et al. 2011a, b, 2013). Notably, Tanguy et al. (1997) have highlighted that the “cicirara” lava

**Fig. 7** Open squares are results from calculations performed using several models. Pressure (a) and temperature (b) estimates were determined by models of Putirka (2008). Melt redox state (c) are calculated following Kress and Carmichael (1991) and France et al. (2010). The melt-water content (d) is derived using the models of Putirka (2005) and Lange et al. (2009).  $^{cpx-melt}Kd_{Fe-Mg}$  and  $^{plg-melt}Kd_{Ab-An}$  values come from regression analyses of Putirka (2008). When not visible, error bars are within symbols

contains plagioclase and clinopyroxene phenocryst cores with an almost homogeneous composition. In this study, the equilibrium condition between clinopyroxene cores and the “cicirara” melt was tested by using the iron-magnesium partitioning model of Putirka (2008). Results suggest that, at the early stage of crystallization, clinopyroxene cores equilibrated with the magma ( $^{cpx-liq}Kd_{Fe-Mg}=0.27\pm 0.03$ ;  $^{cpx-liq}Kd_{Fe-Mg} = ^{cpx}X_{FeO} \times ^{cpx}X_{MgO} / ^{melt}X_{FeO} \times ^{melt}X_{MgO}$ ) and therefore their compositions were used as input data for the most suitable clinopyroxene-based thermobarometers (see the review study by Putirka 2008). The estimates obtained by five different thermometers and barometers produced a range of  $P$ – $T$  conditions (Fig. 7a, b) whose average values are  $P=356\pm 60$  MPa and  $T=1,145\pm 20^\circ\text{C}$  (Fig. 7a, b). Since clinopyroxene cores are in equilibrium with the trachybasaltic melt, their  $Fe^{2+}/Fe^{3+}$  ratios were also used for determining the redox state of magma (Kress and Carmichael 1991), corresponding to the QFM (quartz–fayalite–magnetite) buffer (Fig. 7c). Alternatively, the  $fO_2$  of the “cicirara” melt was estimated by the different partitioning behaviour of ferrous and ferric iron in plagioclase/melt and clinopyroxene/melt pairs (see the model of France et al. 2010). Again, the obtained value was close to the QFM buffer (Fig. 7c) as it is expected for Etnean trachybasaltic magmas (Metrich and Rutherford 1998 and references therein).

The water content of the melt was measured through hygrometers based on plagioclase-liquid equilibrium (Putirka 2005; Lange et al. 2009) and using as input data (1) the pressure ( $356\pm 60$  MPa) calculated by clinopyroxene-based thermobarometers and (2) the equilibrium temperature ( $1,100^\circ\text{C}$ ) of plagioclase experimentally determined for Etnean trachybasaltic liquids (Mollo et al. 2011a). To test the equilibrium condition between plagioclase cores and the melt, we used the Ab–An exchange reaction ( $^{plg-melt}Kd_{Ab-An} = ^{plg}X_{Ab} \times ^{melt}X_{AlO_{1.5}} \times ^{melt}X_{CaO} / ^{plg}X_{An} \times ^{melt}X_{NaO_{0.5}} \times ^{melt}X_{SiO_2}$ ) proposed by Putirka (2008). The equilibrium constant for An–Ab exchange is constrained within two temperature-dependent intervals of  $^{plg-melt}Kd_{Ab-An}=0.10\pm 0.05$  at  $T < 1,050^\circ\text{C}$  and  $^{plg-melt}Kd_{Ab-An}=0.27\pm 0.11$  at  $T > 1,050^\circ\text{C}$  (see Putirka 2008 for further details). Figure 7d shows that  $^{plg-melt}Kd_{Ab-An}$  values calculated for the plagioclase phenocryst cores fall within the equilibrium range of  $0.27\pm 0.11$ . Notably, Mollo et al. (2011a) have experimentally demonstrated that, at the equilibrium temperature of  $1,100^\circ\text{C}$ , the Etnean trachybasaltic magmas have  $^{plg-melt}Kd_{Ab-An}=0.17\pm 0.02$  that is very close to the value of  $0.19\pm 0.02$  measured for our



natural crystals. Results from the model of Putirka (2005) were chosen for the estimate of melt-water content since this model is more suitable for our natural plagioclase–melt pairs (Mollo et al. 2011a). Therefore, the initial water content of the

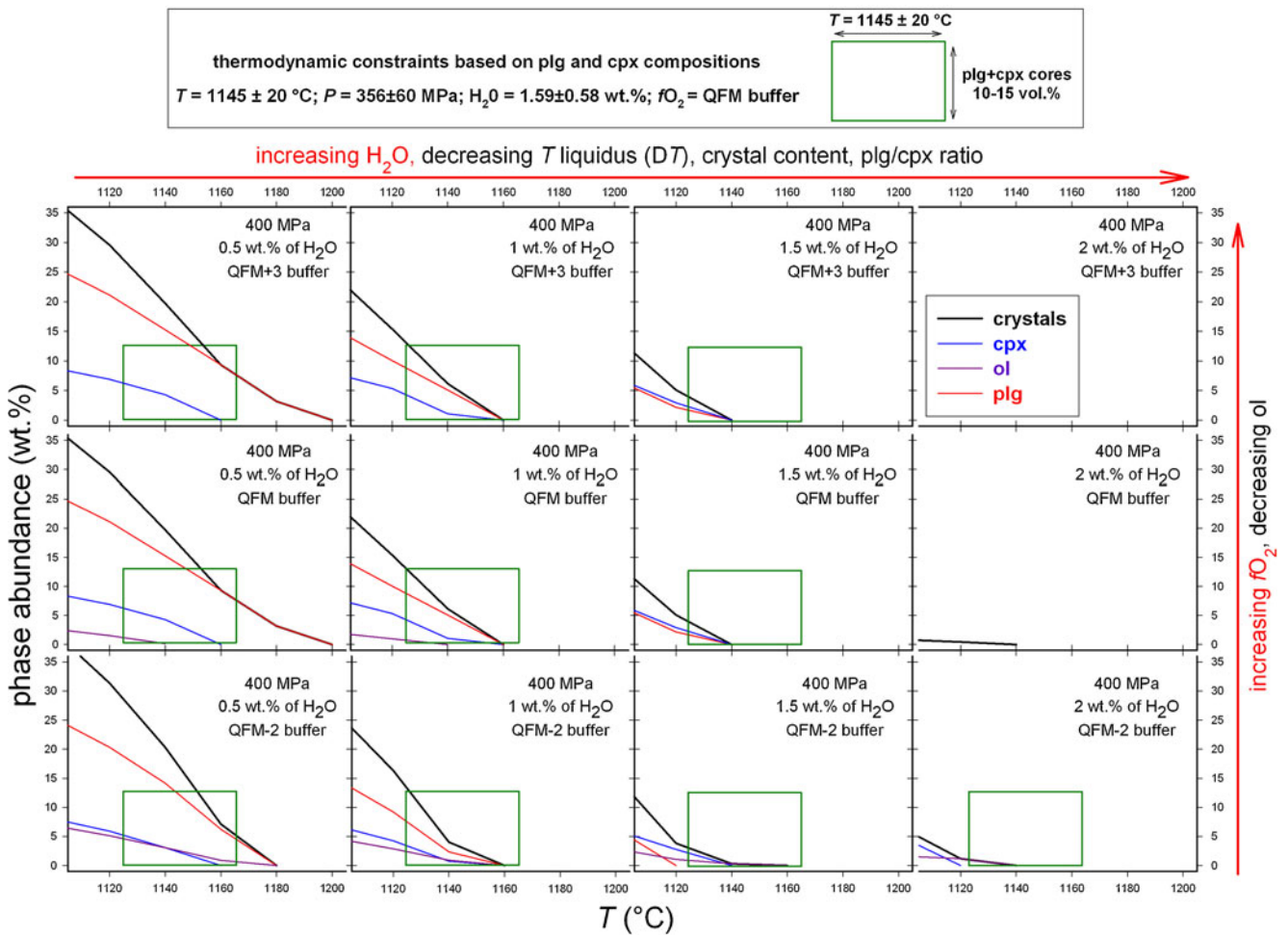
CICG1 “cicirara” melt was determined to be  $1.59 \pm 0.58$  wt.% (Fig. 7d), in agreement with the typical 1–3 wt.% of H<sub>2</sub>O estimated for Etnean magmas (Corsaro and Pompilio 2004).

Figure 8 shows an overview of MELTS (Ghiorso and Sack 1995) simulations performed using as input data (1) the CICG1 bulk composition, (2) H<sub>2</sub>O contents of 0.5, 1, 1.5 and 2 wt.%, (3) buffering conditions of QFM-2, QFM and QFM+3, (4) temperatures from 1,100°C to 1,200°C and (5) 400 MPa of pressure (notably, replicated simulations at 200 MPa do not significantly change the results attained at 400 MPa). The *T–P–H<sub>2</sub>O* conditions estimated using thermometers, barometers and hygrometers are also reported in Fig. 8, together with the total volume of plagioclase and clinopyroxene cores measured for the CCG1 sample. By comparing all the data we observe that the best matching result is that of 1,125–1,165°C, 400 MPa, in presence of 1 wt.% of H<sub>2</sub>O and at the QFM buffer (Fig. 8). Therefore, considering a crustal gradient of 30 MPa/km (Spilliaert et al. 2006), we assume that plagioclase and clinopyroxene cores

formed at 12 km of depth between 1,125°C and 1,165°C. These conditions are also comparable to those discussed in previous studies dealing with thermal gradients beneath Mount Etna volcano (Bonaccorso et al. 2010; Mollo et al. 2011c, 2012a; Heap et al. 2012).

### Crystallization during magma ascent

Clues on the solidification process of the CICG1 magma during its ascent to the surface can be obtained through the behavior of volatile species at variable pressures. To do this, we used the SolEx code (Witham et al. 2012) to perform two simulations using as input data (1) the maximum amounts of CO<sub>2</sub>, S and Cl measured at Mount Etna (Spilliaert et al. 2006; Collins et al. 2009) and (2) water contents of 1 and 3 wt.%, respectively. The temperature was fixed at 1,150°C, and the pressure started from 400 MPa (about 12 km of depth). During magma ascent a conservative initial H<sub>2</sub>O



**Fig. 8** Models of CCG1 crystal phase assemblages performed using MELTS code (Ghiorso and Sack 1995) at  $T=1,100\text{--}1,200^\circ\text{C}$ ,  $\text{H}_2\text{O}=0.5\text{--}2$  wt.%,  $\text{QFM-2} < f\text{O}_2 < \text{QFM+3}$ . Estimates of crystallization conditions obtained by compositions of plagioclase and clinopyroxene

cores and their relative proportions are also reported. These data indicate that the crystallization of the CICG1 magma began at 1,125–1,160°C, 0.4 GPa, QFM buffer and 1 wt.% of H<sub>2</sub>O

content of 1 wt.% should be exsolved at about 40 MPa (a depth of about 1 km) (Fig. 9). Notably, at the lowest crystallization temperature (1,125°C) inferred for plagioclase and clinopyroxene cores (Fig. 8), H<sub>2</sub>O is exsolved from the melt at crustal depths <1 km (Fig. 9). Therefore, crystallization induced by H<sub>2</sub>O exsolution during magma ascent can occur only at shallow depths, if the magma has a slow ascent rate. Additionally, solubility data indicate that CO<sub>2</sub> degassing may contribute to increase the liquidus temperature of the melt, causing resorption of plagioclase (and possibly clinopyroxene) cores until 1 km of depth (Fig. 9).

The total amount of phenocrysts and microphenocrysts in our two sub-samples is 40 and 43 vol.% (Table 3), respectively. These crystals are generally interpreted as originating from massive crystallization in volcanic reservoirs and conduits (Murphy et al. 2000; Couch et al. 2003). However, we have determined that the crystal content of the CICG1 magma at 12 km of depth is only 10–15 vol.%. This implies two possible scenarios: (1) about 30 vol.% of crystals solidified in the last 1 km beneath the surface due to H<sub>2</sub>O degassing or (2) microphenocrysts crystallized after the

eruption. Scenario (1) would imply that the CICG1 lava is erupted with a high crystal content ( $\geq 40$  vol.%), hampering the formation of a *pahoehoe* type lava crust. Conversely, scenario (2) is more likely and can be demonstrated by comparing cumulative size frequency and plagioclase CSD data, i.e., the three log-linear parts of the CSD curve obtained for a crystal content of 78–79 vol.% (Table 3). These data are plotted in Fig. 10, together with crystal limits required to develop both *pahoehoe* and *aa* morphologies and additional data on size frequencies from historical *aa* lavas. The three log-linear parts of the CSD curve indicate that at least three different solidification conditions were recorded by the textural evolution of plagioclase (Figs. 6 and 10). The increasing slope of the CSD log-linear trends, i.e., low, intermediate and high slopes (red, blue and green lines of Fig. 10) for plagioclase sizes >1, 0.1–1 and <0.1 mm (Fig. 6), highlight an increasing degree of undercooling and a crystallization behavior driven by a high crystal nucleation rate (Armienti 2008; Hammer 2008). As already demonstrated by Armienti et al. (1994a) for the 1991–1993 Etnean *aa* lavas, the intermediate CSD slope is

**Fig. 9** Solubility models of volatiles in the CICG1 magma as a function of pressure, at 1,150°C and NNO+0.5 buffer. The trends depicted at H<sub>2</sub>O=1 wt.% are representative for the ascent of the CICG1 magma

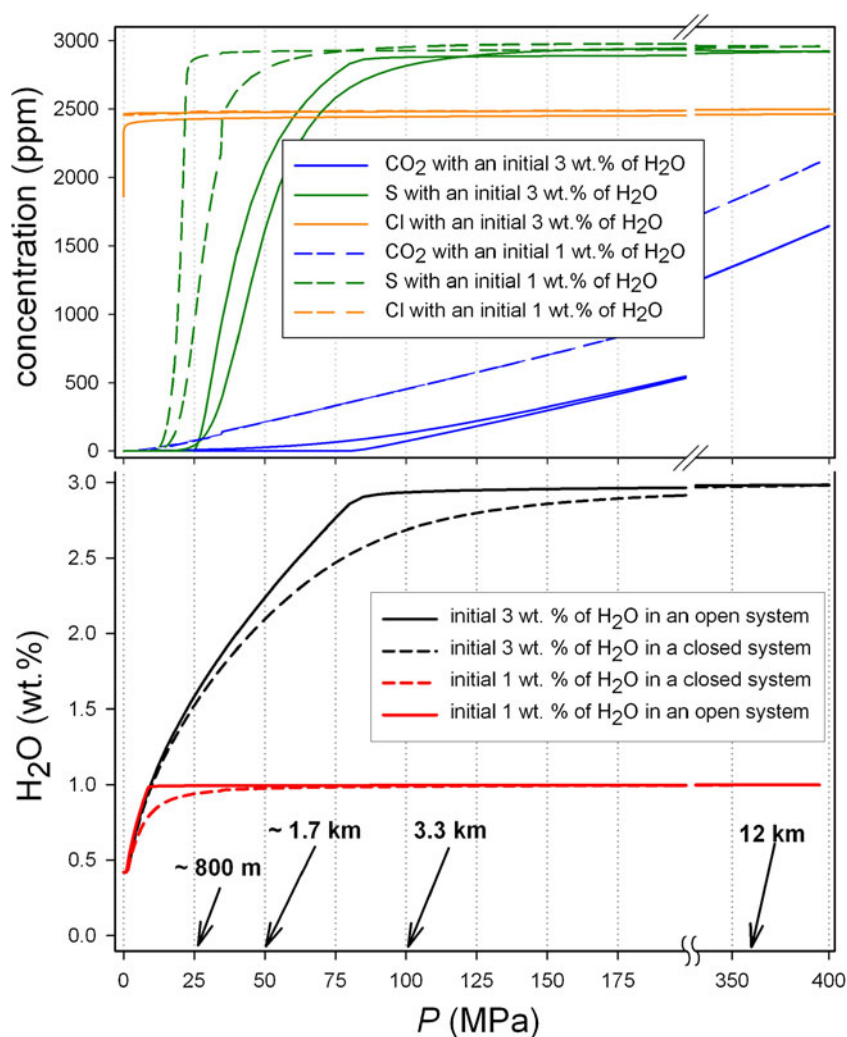
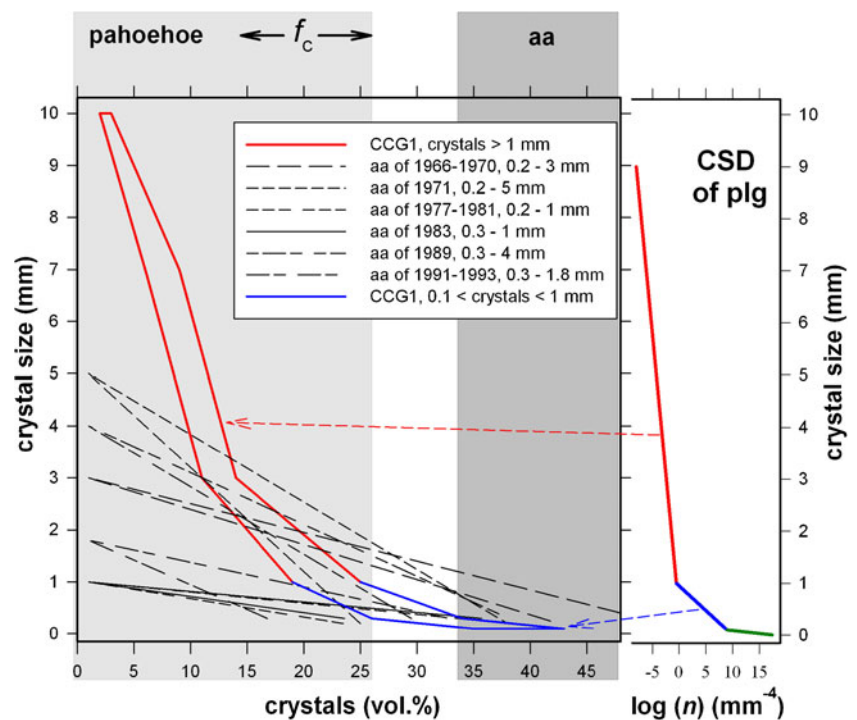


**Fig. 10** Cumulative size frequency trends (thick lines) of the CCG1 sub-samples compared with those available in literature for *aa* lavas: 1966–1971 (Tanguy 1973), 1977–1983 (Tanguy and Clocchiati 1984), 1983 (Armienti et al. 1984; Fazzetta and Romano 1984), 1989 (Kilburn and Guest 1993), and 1991–1993 (Armienti et al. 1994a, b). The light- and dark-grey boxes show the maximum and minimum crystal contents of Hawaiian *pahoehoe* and *aa* lavas, respectively (Hoover et al. 2001). The theoretical range for the development of a critical yield strength ( $\Phi_c$ ) is also reported for a suspension with randomly oriented solid particles with rectangular (1:2:2/5) shape (Saar et al. 2001). The right diagram shows a schematic CSD plot of plagioclase from Fig. 6



due to the crystallization of microphenocrysts during magma ascent in the conduit. However, this interpretation cannot be used for the log-linear part of the plagioclase CSD of the CCG1 lava (see the blue segment in Fig. 10), otherwise we should conclude that this lava was erupted and flowed with a crystal content of 40–43 vol.% (Table 3 and Fig. 10) that is definitively in contrast with the *pahoehoe* morphology. Therefore, only plagioclase crystals with a length >1 mm and belonging to CSD curves with the lowest slope (Fig. 6) should have crystallized at pre-eruptive conditions. Indeed, different solidification conditions for the *pahoehoe* CCG1 lava and the *aa* lavas erupted in the last decades at Mount Etna volcano are pointed out by their different cumulative size frequency trends (Fig. 10). With respect to Etnean *aa* lavas, the cumulative size frequency of CCG1 has a high slope at larger crystal sizes (>1 mm). This high slope suggests a decreasing nucleation density due to lower degrees of undercooling before eruption. Such a feature finds an interesting analogue in the results of Sato (1995), who investigated the *aa* and *pahoehoe* morphologies of the Izu–Oshima lavas. Sato (1995) showed that when magma experiences a rapid undercooling due to H<sub>2</sub>O exsolution, *aa* lavas with a high crystal density are favoured with respect to *pahoehoe* types; notably, the opposite occurs at low degrees of undercooling, even for similar magma compositions. The total content of phenocrysts and microphenocrysts in CCG1 sub-samples is 40 and 43 vol.%, respectively. According to data reported in Fig. 10, *pahoehoe* morphology can develop only for crystal content lower than 26 vol.%. Since 10–15 vol.% of phenocryst cores formed at a depth of

12 km, only 11 vol.% of phenocrysts may have crystallized during magma ascent (Table 3).

The CSD segment obtained for plagioclases >1 mm corresponds to two main trends of the cumulative size frequency (see red lines in the cumulative size frequency diagram of Fig. 10), underlining slightly different growth styles under intratelluric conditions. On the contrary, the near horizontal CSD slope for plagioclases >1 mm (Fig. 6) testifies to a very low nucleation rate, practically the same as that of larger crystals. We infer that, to maintain the same nucleation rate, while 11 vol.% of crystallization takes place during magma ascent, it is required that the nucleation develops heterogeneously around the early-formed plagioclase (and clinopyroxene) cores. This is supported by the agglomeration features observed for large plagioclases (Figs. 3c, d, 4 and 5). Indeed, heterogeneous nucleation and crystal agglomeration have been observed in several experimental studies (Pupier et al. 2008; Iezzi et al. 2011; Mollo et al. 2011a, 2012b) demonstrating that, under kinetically controlled conditions, smaller crystals heterogeneously nucleate and agglomerate onto larger ones. Notably, in the case of plagioclase, similar mechanisms produce An-rich cores surrounded by An-poor rims (Iezzi et al. 2011).

### Crystallization after eruption

Since the amount of phenocrysts formed before eruption was no more than 21–25 vol.%, then the majority of the crystallization occurred at subaerial conditions after the

formation of the rapidly cooled *pahoehoe* crust. Such a process is not rare. For example, massive crystallization (>50 vol.%) during lava emplacement has been reported by Crisp et al. (1994) for the Mauna Loa lava of 1984. In the case of the Hawaiian magmas, the occurrence of olivine, orthopyroxene and clinopyroxene as liquidus phases enriches the residual melt in Si and Al; consequently, the liquid becomes reluctant to nucleate and more prone to vitrify (Sparks et al. 2000; Iezzi et al. 2008, 2009, 2011). In contrast, the higher subaerial crystallization of the “cicirara” lava (>75 vol.%) is due to the early formation of a large amount of plagioclases that enrich the melt in Fe and Mg, triggering the nucleation of olivine, clinopyroxene and titanomagnetite crystals.

The intermediate (0.1–1 mm) and high (<0.1 mm) slopes of the plagioclase CSD reported in Fig. 6 (see also blue and green lines in Fig. 10) indicate different solidification behaviors; notably, two crystallization events at subaerial conditions are also observable for the clinopyroxene (Fig. 6). We infer that H<sub>2</sub>O did not exsolve completely during rapid magma ascent, as in the case of lateral eruptions at Mount Etna volcano (Metrich and Rutherford 1998). Our interpretation will also give reason for the presence of a significant amount of bubbles only in the uppermost part of the CIG1 lava (0.1 m below the *pahoehoe* crust). It follows that the intermediate slope of plagioclase CSD reflects the formation of crystals driven by water loss during lava solidification. This crystallization event was not recorded by the surface morphology of the lava flow because it rapidly solidified under fast cooling rates. The absence of widespread fractures testifies to a low strain rate unable to disrupt the *pahoehoe* carapace (Kilburn 2004), perhaps suggesting a low effusion rate. Conversely, the high CSD slope for plagioclases <0.1 mm indicates that, after degassing, a large amount of crystals rapidly formed in response to a fast undercooling (Figs. 6 and 10). In fact, the high concentrations of Fe in plagioclase (Table 2) and Al in clinopyroxene (Table 2) indicate a massive crystallization of microlites under kinetically controlled conditions (Mollo et al. 2010, 2011a, b, 2012c) and temperatures much higher than 680°C, i.e., the glass transition of Etnan trachybasaltic melts (Iezzi et al. 2009). The low difference in plagioclase phenocryst content (Table 3) measured for the two CIG1 sub-samples, suggests the presence of two slightly different cooling paths as a function of the distance from the uppermost part of the lava flow (cf. Mollo et al. 2012b).

### Rheological path of the CIG1 “cicirara”

In Fig. 11, we summarize previous results and provide the rheological path for the CIG1 “cicirara” lava. The apparent viscosity of the suspension (melt+crystals) was computed

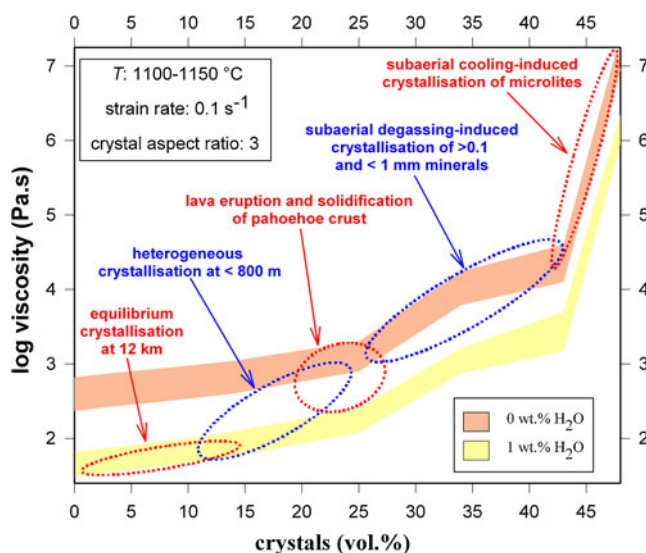


**Fig. 11** The rheological path of the CIG1 magma from the magmatic reservoir to the final emplacement condition

using the model of Vona et al. (2011) on the basis of the amount and shape of the crystals (Table 3); whereas, the composition of the residual melt was estimated by mass balances and its viscosity was determined using the model of Giordano et al. (2008). For the calculation, we considered an average strain rate of  $0.1 \text{ s}^{-1}$  (Hon et al. 2003), anhydrous and hydrous (H<sub>2</sub>O=1 wt.%) conditions, and a temperature interval of 1,100–1,150°C. Results indicate that the CIG1 magma was characterized by an initial low viscosity of 2 log Pas. Under hydrous conditions, when magma was rising in the last 1,000 m of the conduit, the viscosity slightly increased due to (1) the partial exsolution of water and (2) the onset of heterogeneous crystallization of phenocryst rims. At the vent, the bulk viscosity did not exceed 3 log Pas (Fig. 11) favouring the formation of a *pahoehoe* carapace. Since the lava completely degassed during flow, 45 vol.% of crystals formed and the lava viscosity increased to 4.5 log Pas. The massive crystallization of microlites occurred at the final stage of the solidification path, significantly increasing the viscosity of the suspension (Fig. 11).

### Conclusions

The crystallization behaviour that we have outlined in this study is controlled by the efficiency of degassing, which is in turn related to the velocity of magma ascent (Ferlito and Lanzafame 2010). At Mount Etna, the last portion of the feeding system is an open-conduit persistently filled with magma (Ferlito et al. 2011). The most frequent eruptive activity occurs at subterminal craters (above 3,000 ma.s.l.) and along fractures related to these structures (Corsaro et al.

2009). Since the magma in the uppermost conduit is efficiently degassed, the degree of undercooling significantly increases (Sato 1995) favouring the formation of a large amount of nuclei within the conduit (Armienti 2008). Thus, abundant crystallization takes place before eruption and the erupted lavas develop into *aa* flows. This scenario is depicted by the cumulative size frequency diagram (Fig. 10). Similar conclusions can be drawn considering the CSD data of plagioclase and clinopyroxene in *aa* lavas of Armienti et al. (1994a). Indeed, the low and intermediate slopes of the three log-linear CSD portions of *aa* lavas clearly reflect intratelluric crystallization conditions (Armienti et al. 1994a, 1997). In contrast, *pahoehoe* “cicirara” lavas (e.g., the CIGC1 trachybasalt) show a different cumulative size frequency trend. Importantly, only the CSD log-linear segment of large plagioclase phenocrysts mirrors crystallization conditions before eruption (Fig. 10). This implies that *pahoehoe* lavas are due to magma ascent conditions characterized by a low degree of undercooling that can only occur when the magma ascent is fast. Fast ascent rates could be associated with tectonically controlled fissures that provide conduits for lateral eruptions where degassing is much lower than open conduit conditions typical of most of the Etnean lava emissions.

Similar investigations as that reported here on the relationship among textural, micro-chemical and surface features of several *pahoehoe* “cicirara” lavas erupted in the last thousands of years (cf. Table 1) are currently being undertaken by our group; the results of these new studies will potentially allow researchers to constrain the different magma withdrawal processes at Mount Etna volcano. Finally, we point out that the size limits among phenocrysts, microphenocrysts and microlites can be used as useful petrological indicators only after a quantitative investigation of the mineral textural features (cf. Kuritani 1999).

**Acknowledgments** We appreciate the constructive comments of M. Patrick, P. Armienti and M. D. Higgins. This study was supported by the “Fondi Ateneo of the University G. d’Annunzio” and the PRIN project “Experimental determination of the glass-forming ability (GFA), nucleation and crystallization of natural silicate melts” awarded to G. Iezzi. S. Mollo was supported by the ERC Starting Grant No. 259256 GLASS project.

## References

- Armienti P (2008) Decryption of igneous rock textures: crystal size distributions tools. In: Putirka KD, Tepley FJ (eds) Minerals, inclusions and volcanic processes, vol. 69, Reviews in mineralogy and geochemistry. Mineralogical Society of America, Chantilly, pp 623–649
- Armienti P, Barberi F, Innocenti F, Pompilio M, Romano R, Villari L (1984) Compositional variation in the 1983 and other recent Etnean lavas: insights on the shallow feeding system. Bull Volcanol 47:995–1007
- Armienti P, Pareschi MT, Pompilio M, Innocenti F (1994a) Effects of magma storage and ascent on the kinetics of crystal growth: the case of the 1991–1993 Mt. Etna eruption. Contrib Mineral Petrol 115:402–414
- Armienti P, Clocchiatti R, D’Orazio M, Innocenti F, Petrini R, Pompilio M, Tonarini S, Villari L (1994b) The long-standing 1991–1993 Mount Etna eruption: petrography and geochemistry of lavas. Acta Vulcanol 4:15–28
- Armienti P, Pareschi MT, Pompilio M (1997) Lava textures and time scales of magma storage at Mt. Etna. Acta Vulcanol 9:1–5
- Bonaccorso A, Currenti G, Del Negro C, Boschi E (2010) Dike deflection modelling for inferring magma pressure and withdrawal, with application to Etna 2001 case. Earth Planet Sci Lett 293 (1–2):121–129
- Branca S, Coltelli M, Groppelli G, Lentini F (2011) Geological map of Etna volcano, 1:50000 scale. Ital J Geosci 130:265–291
- Cashman KV, Kauahikaua JP, Thornber C (1999) Cooling and crystallization of lava in open channels, and the transition of pahoehoe lava to a’a. Bull Volcanol 61:306–323
- Chester DK, Duncan AM, Guest JE, Kilburn CJR (1985) Mount Etna: the anatomy of a volcano. Chapman and Hall, London, pp 65–123
- Collins SJ, Pyle DM, Maclennan J (2009) Melt inclusions track pre-eruption storage and dehydration of magmas at Etna. Geology 6:571–574
- Corsaro RA, Pompilio M (2004) Dynamics of magmas at Mount Etna. In: Bonaccorso A, Calvari S, Coltelli M, Del Negro C, Falsaperla S (eds) Mt. Etna volcano laboratory, vol. 143. AGU Geophysical Monograph Series, Washington, pp 91–110
- Corsaro RA, Metrich N, Allard P, Andronico D, Miraglia L, Fourmentraux C (2009) The 1974 flank eruption of Mount Etna: an archetype for deep dike-fed eruptions at basaltic volcanoes and a milestones in Etna’s recent history. J Geophys Res B07204. doi:10.1029/2008JB006013
- Couch S, Sparks RSJ, Carroll MR (2003) The kinetics of degassing-induced crystallisation at Soufriere Hills volcano, Montserrat. J Petrol 44:1477–1502
- Crisp J, Cashman CK, Bonini JA, Hougén SB, Pieri DC (1994) Crystallization history of the 1984 Mauna Loa lava flow. J Geophys Res 99:7177–7198
- Del Gaudio P, Mollo S, Ventura G, Iezzi G, Taddeucci J, Cavallo A (2010) Cooling rate-induced differentiation in anhydrous and hydrous basalts at 500 MPa: implications for the storage and transport of magmas in dikes. Chem Geol 270:164–178
- Fazzetta G, Romano R (1984) The 1983 Etna eruption: event chronology and morphological evolution of the lava flow. Bull Volcanol 47:1079–1096
- Ferlito C, Lanzafame G (2010) The role of supercritical fluids in the potassium enrichment of magmas at Mount Etna volcano (Italy). Lithos 119:642–650
- Ferlito C, Viccaro M, Nicotra E, Cristofolini R (2011) Regimes of magma recharge on the eruptive behaviour during the period 2001–2005 at Mt. Etna volcano. Bull Volcanol 74(2):533–543
- France L, Koepke J, Ildefonse B, Cichy SB, Deschamps F (2010) Hydrous partial melting in the sheeted dike complex at fast spreading ridges: experimental and natural observations. Contrib Mineral Petrol 5:683–704
- Ghiorso MS, Sack RO (1995) Chemical mass-transfer in magmatic processes IV. A revised and internally consistent thermodynamic model for the interpolation and extrapolation of liquidus-solid equilibria in magmatic systems at elevated temperatures and pressures. Contrib Mineral Petrol 119:197–212
- Giordano D, Russell JK, Dingwell DB (2008) Viscosity of magmatic liquids: a model. Earth Planet Sci Lett 271:123–134
- Guest JE, Wood C, Greeley R (1984) Lava tubes, terraces and megatumuli on the 1614–24 pahoehoe lava flowfield, Mount Etna, Sicily. Bull Volcanol 47:635–648

- Guest JE, Duncan AM, Stofan ER, Anderson SW (2012) Effect of slope on the development of pahoehoe flow fields: evidence from Mount Etna. *J Volcanol Geotherm Res* 219–220:52–62
- Hammer JE (2008) Experimental studies of the kinetics and energetics of magma crystallization. In: Putirka KD, Tepley FJ (eds) *Minerals, inclusions and volcanic processes*, vol. 69, Reviews in mineralogy and geochemistry. Mineralogical Society of America, Chantilly, pp 9–59
- Heap MJ, Mollo S, Vinciguerra S, Lavallée Y, Hess KU, Dingwell DB, Baud P, Iezzi G (2012) Thermal weakening of the carbonate basement under Mt. Etna volcano (Italy): implications for volcano instability. *J Volcanol Geotherm Res* 250:42–60. doi:10.1016/j.jvolgeores.2012.10.004
- Higgins MD (2000) Measurement of crystal size distributions. *Am Mineral* 85:1105–1116
- Higgins MD (2006) *Quantitative textural measurements in igneous and metamorphic petrology*. Cambridge University Press, Cambridge
- Hon K, Gansecki C, Kauahikaua J (2003) The transition from a'a to pahoehoe crust on flows emplaced during the Pu'u O'o-Kupaianaha eruption. *US Geol Surv Prof Pap* 1676:89–104
- Hoover SR, Cashman KV, Manga M (2001) The yield strength of subliquidus basalts: experimental results. *J Volcanol Geotherm Res* 107:1–18
- Hughes JW, Guest JE, Duncan AM (1990) Changing styles of effusive eruption on Mount Etna since AD 1600. In: Ryan MP (ed) *Magma transport and storage*. Wiley, London, pp 385–405
- Iezzi G, Ventura G (2005) The kinematics of lava flows inferred from the structural analysis of enclaves: a review. In: Manga M, Ventura G (eds) *Kinematics and dynamics of lava flows*. Geological Society of America, Boulder, pp 15–28
- Iezzi G, Mollo S, Ventura G, Cavallo A, Romano C (2008) Experimental solidification of anhydrous latitic and trachytic melts at different cooling rates: the role of nucleation kinetics. *Chem Geol* 253:91–101
- Iezzi G, Mollo S, Ventura G (2009) Solidification behaviour of natural silicate melts and volcanological implications. In: Lewis N, Moretti A (eds) *Volcanoes: formation, eruptions and modeling*. Nova publishers, New York, pp 127–151
- Iezzi G, Mollo S, Torresi G, Ventura G, Cavallo A, Scarlato P (2011) Experimental solidification of an andesitic melt by cooling. *Chem Geol* 283(3–4):261–273
- Kilburn CRJ (2004) Fracturing as a quantitative indicator of lava flow dynamics. *J Volcanol Geotherm Res* 132:209–224
- Kilburn CRJ, Guest JE (1993) Aa lavas of Mount Etna, Sicily. In: Kilburn CRJ (ed) *Active lavas*. UCL Press, London, pp 73–106
- Kress VC, Carmichael ISE (1991) The compressibility of silicate liquids containing  $Fe_2O_3$  and the effect of composition, temperature, oxygen fugacity and pressure on their redox states. *Contrib Mineral Petrol* 108:82–92
- Kuritani T (1999) Phenocryst crystallization during ascent of alkali basalt magma at Rishiri Volcano, northern Japan. *J Volcanol Geotherm Res* 88:77–97
- Lange RA, Frey HM, Hector J (2009) A thermodynamic model for the plagioclase-liquid hygrometer/thermometer. *Am Mineral* 94:494–506
- Metrich N, Rutherford MJ (1998) Low pressure crystallization paths of  $H_2O$ -saturated basaltic-hawaiitic melts from Mt Etna: implications for open-system degassing of basaltic volcanoes. *Geochim Cosmochim Acta* 62:1195–1205
- Mollo S, Del Gaudio P, Ventura G, Iezzi G, Scarlato P (2010) Dependence of clinopyroxene composition on cooling rate in basaltic magmas: implications for thermobarometry. *Lithos* 118:302–312
- Mollo S, Putirka K, Iezzi G, Del Gaudio P, Scarlato P (2011a) Plagioclase-melt (dis)equilibrium due to cooling dynamics: implications for thermometry, barometry and hygrometry. *Lithos* 125:221–235
- Mollo S, Lanzafame G, Masotta M, Iezzi G, Ferlito C, Scarlato P (2011b) Cooling history of a dike as revealed by mineral chemistry: a case study from Mt. Etna volcano. *Chem Geol* 288:39–52
- Mollo S, Vinciguerra S, Iezzi G, Iarocci A, Scarlato P, Heap MJ, Dingwell DB (2011c) Volcanic edifice weakening via devolatilization reactions. *Geophys J Int* 186:1073–1077. doi:10.1111/j.1365-246X.2011.05097.x
- Mollo S, Heap MJ, Iezzi G, Hess K-U, Scarlato P, Dingwell DB (2012a) Volcanic edifice weakening via decarbonation: a self-limiting process? *Geophys Res Lett* 39:L15307. doi:10.1029/2012GL052613,2012
- Mollo S, Iezzi G, Ventura G, Cavallo A, Scarlato P (2012b) Heterogeneous nucleation mechanisms and formation of metastable phase assemblages induced by different crystalline seeds in a rapidly cooled andesitic melt. *J Non-Cryst Solids* 358:1624–1628
- Mollo S, Misiti V, Scarlato P, Soligo M (2012c) The role of cooling rate in the origin of high temperature phases at the chilled margin of magmatic intrusions. *Chem Geol*. doi:10.1016/j.chemgeo.2012.05.029
- Mollo S, Scarlato P, Lanzafame G, Ferlito C (2013) Deciphering lava flow post-eruption differentiation processes by means of geochemical and isotopic variations: A case study from Mt. Etna volcano. *Lithos* 162–163:115–127. doi:10.1016/j.lithos.2012.12.020
- Morgan DJ, Jerram DA (2006) On estimating crystal shape of crystal size distribution analysis. *J Volcanol Geotherm Res* 154:1–7
- Murphy MD, Sparks RSJ, Barclay J, Carroll MR, Brewer TS (2000) Remobilization of andesite magma by intrusion of mafic magma at the Soufriere Hills Volcano, Montserrat, West Indies. *J Petrol* 41:21–42
- Nicotra E, Viccaro M (2012) Unusual magma storage conditions at Mt. Etna (Southern Italy) as evidenced by plagioclase megacryst-bearing lavas: implications for the plumbing system geometry and summit caldera collapse. *Bull Volcanol* 74:795–825. doi:10.1007/s00445-011-0566-9
- Pupier E, Duchene S, Toplis MJ (2008) Experimental quantification of plagioclase crystal size distribution during cooling of a basaltic liquid. *Contrib Mineral Petrol* 155:555–570
- Putirka K (2005) Igneous thermometers and barometers based on plagioclase+liquid equilibria: test of some existing models and new calibrations. *Am Mineral* 90:336–346
- Putirka K (2008) Thermometers and barometers for volcanic systems. In: Putirka KD, Tepley F (eds) *Minerals, inclusions and volcanic processes*, vol. 69, Reviews in mineralogy and geochemistry. Mineralogical Society of America, Chantilly, pp 61–120
- Saar MO, Manga M, Cashman KV, Fremouw S (2001) Numerical models of the onset of yield strength in crystal-melt suspensions. *Earth Planet Sci Lett* 187:367–379
- Sato H (1995) Textural difference between pahoehoe and aa lavas of Izu-Oshima volcano, Japan: an experimental study on population density of plagioclase. *J Volcanol Geotherm Res* 66:101–113
- Soule SA, Cashman KV (2005) Shear rate dependence of the pahoehoe-to-a'a transition: Analog experiments. *Geology* 33:361–364
- Sparks RSJ, Murphy MD, Lejeune AM, Watts RB, Barclay J, Young SR (2000) Control on the emplacement of the andesite lava dome of the Soufriere Hills volcano, Montserrat by degassing-induced crystallization. *Terra Nova* 12:14–20
- Spilliaert N, Allard P, Metrich N, Sobolev AV (2006) Melt inclusion record of the conditions of ascent, degassing, and extrusion of volatile-rich alkali basalt feeding the powerful 2002 flank eruption of Mount Etna (Italy). *J Geophys Res* 111:B04203
- Tanguy JC (1973) The 1971 Etna eruption: petrography of the lavas. *Philos Trans R Soc Lond* 274:45–53
- Tanguy JC, Clocchiati R (1984) The Etna lavas, 1977–1983: petrology and mineralogy. *Bull Volcanol* 47:879–894
- Tanguy JC, Condomines M, Kieffer G (1997) Evolution of the Mount Etna magma: constraints on the present feeding system and eruptive mechanism. *J Volcanol Geotherm Res* 75:221–250
- Vona A, Romano C, Dingwell DB, Giordano D (2011) The rheology of crystal-bearing basaltic magmas from Stromboli and Etna. *Geochim Cosmochim Acta* 75:3214–3236
- Witham F, Blundy J, Kohn SC, Lesne P, Dixon J, Churakov SV, Botcharnikov R (2012) SolEx: a model for mixed COHSL-volatile solubilities and exsolved gas compositions in basalt. *Comput Geosci* 45:87–97